Supporting Information for:

A Double-Strip Plasmonic Waveguide Coupled to an Electrically Driven Nanowire LED

You-Shin No, Jae-Hyuck Choi, Ho-Seok Ee, Min-Soo Hwang, Kwang-Yong Jeong,

Eun-Khwang Lee, Min-Kyo Seo, Soon-Hong Kwon, and Hong-Gyu Park

This file includes:

Methods

Supplementary Figures S1 – S6

Methods

Device fabrication. The NW arrays in Figure 2A were fabricated using (p-$Al_{0.45}Ga_{0.55}As$)/(p-$Al_{0.6}Ga_{0.4}As$)/(i-AlGaInP/InGaP)/(n-$Al_{0.6}Ga_{0.4}As$)/(n-$Al_{0.45}Ga_{0.55}As$)/(n-GaAs)/(n-$Al_{0.96}Ga_{0.04}As$)/(n-GaAs substrate) wafer structure. Due to a substantial difference in composition between the n-GaAs and n-$Al_{0.96}Ga_{0.04}As$ layers, the NWs can be broken easily and separated from the substrate in the sonication process. The detailed fabrication procedures after the dispersion of NWs onto SiO_2 substrate are shown in Figure S1 in Supporting Information.

Optical measurements. A current pulse with a width of 100 ns and a period of 1 μs was injected into the NW LED using a pulse generator (RIGOL DG4162). The light emitted/scattered from the NW LED and the plasmonic waveguide was collected by a x50 long-working-distance objective lens with a numerical aperture of 0.55, and focused onto either a CCD camera (PIXIS 400B) or a spectrometer. To measure polarization-resolved images and spectra, a linear polarizer was placed in front of the CCD camera or spectrometer.

FDTD calculations. In the FDTD simulations, metals were modeled by Drude-Lorentz modeling, which can represent dispersive materials over a wide spectral range:[S1]

$$\varepsilon(\omega) = \varepsilon_\infty - \frac{\omega_D^2}{\omega^2 + i\gamma_D\omega} + \frac{\Delta\varepsilon_L\omega_L^2}{\omega_L^2 - \omega^2 - i\gamma_L\omega}$$

in which ε_∞ is the background dielectric constant at infinite frequency, ω_D and γ_D are the electron plasma frequency and damping constant of Drude term, respectively, and $\Delta\varepsilon_L$, ω_L and γ_L are the change in relative permittivity, the undamped frequency and damping constant of Lorentz term, respectively. The plasma and collision frequencies were obtained by fitting the measured refractive indices and extinction coefficients of gold and chromium over the

wavelength range, 700 - 1250 nm.[S2] For gold, only Drude term was used ($\Delta\varepsilon_L$=0), and the parameters used in the simulation were ε_∞=7.26119, ω_D=8.47319 $\hbar^{-1}$ eV, and γ_D=0.0290695 $\hbar^{-1}$ eV, where $\hbar$ is the reduced Planck constant. The parameters of chromium were ε_∞=1.01523, ω_D=5.62522 $\hbar^{-1}$ eV, ω_L=1.98172 $\hbar^{-1}$ eV, γ_D=0.272264 $\hbar^{-1}$ eV, γ_L=3.20969 $\hbar^{-1}$ eV, and $\Delta\varepsilon_L$=47.2679. The refractive indices of GaAs NW and SiO_2 were set to 3.34 and 1.45, respectively.[S2] To calculate the dispersion curves of SPP waveguide modes (Figure S3), a periodic boundary condition was used along the y-direction, and perfectly matched layers were applied at the other boundaries of the calculation domain with a size of 1.23 x 1.60 μm^2 and a spatial resolution of 5 nm. The chromium layer with a thickness of 5 nm was introduced in the plasmonic waveguide, between the gold layer and substrate. To calculate the Poynting vector distributions (Figures 4C-E and S4), we performed three-dimensional FDTD simulation, in which the domain size of 5.00 x 43.50 x 3.50 μm^3 and a spatial resolution of 10 nm were used. In this case, the thickness of the chromium layer in the plasmonic waveguide was set to 10 nm.

References

(S1) Taflove, A.; Hagness, S. C. *Computational electrodynamics: The finite-difference time-domain method*; Artech House: 2000.

(S2) Lide, D. R. *CRC handbook of chemistry and physics: a ready-reference book of chemical and physical data*, 88th ed. (CRC Press, 2008).

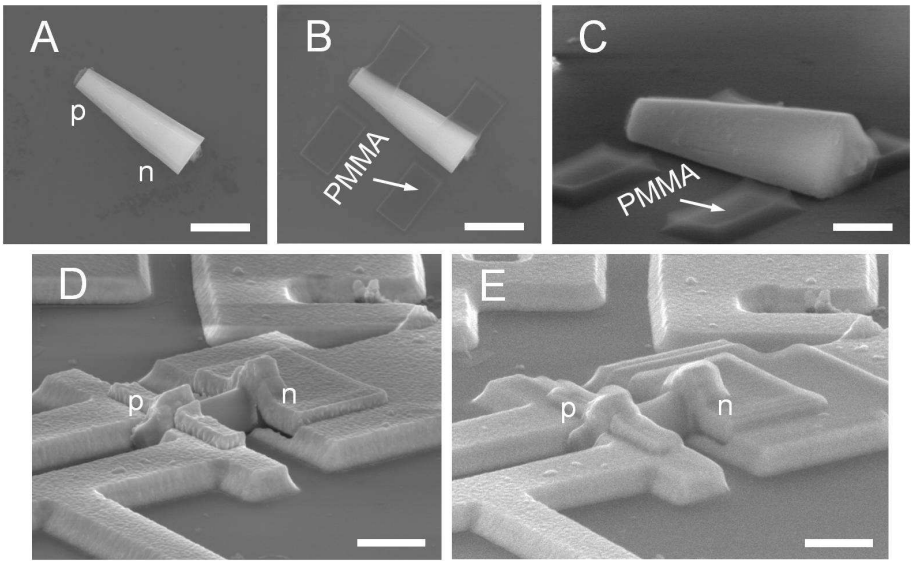

Figure S1. Fabrication procedure of an integrated plasmonic device. (A) SEM image of a top-down-fabricated GaAs NW which was dispersed on SiO_2 substrate. The scale bar is 1 μm. (B) Four PMMA patches were fabricated near the two ends of the NW using EBL. These 200-nm-thick cross-linked PMMA patches are useful to reduce the height difference between the NW and the substrate. The scale bar is 1 μm. (C) Tilted SEM image of (B). The scale bar is 500 nm. (D) 5-nm-thick chromium and 400-nm-thick gold were deposited on both ends of the NW. The conformal deposition of metals was achieved despite relatively large height of the NW, due to the angled sidewall of the NW with a triangular cross-section as well as the PMMA patches. The scale bar is 1 μm. (E) The electron-beam induced deposition (EBID) of platinum and carbon compound material can be applied to remove cracks on the metal electrodes and improve electrical contact between the NW and the electrodes. The scale bar is 1 μm.

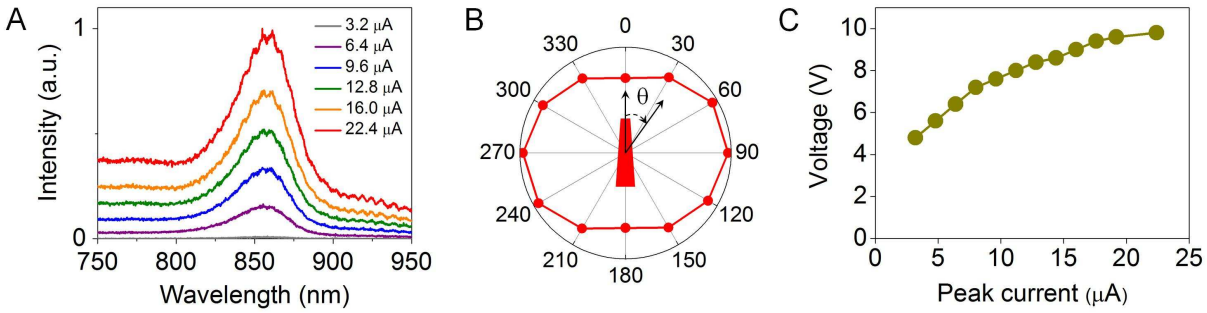

Figure S2. Optical and electrical characteristics of an electrically driven NW LED. (A) EL spectra measured from the NW LED by injection of current pulses with a 10% duty cycle but different peak values. The central wavelength of the spectra is ~850 nm, which indicates the light emission from the n-GaAs layer of the NW. The slit width of the spectrometer was wider than the one in Figure 2D. (B) Output intensity of the NW LED measured as a function of the polarization angle, θ, between the NW axis and the transmission axis of the linear polarizer. No preferred direction of polarization was observed from the NW LED. (C) Measured current-voltage characteristic of the NW LED. The device resistance of ~210 kΩ was estimated.

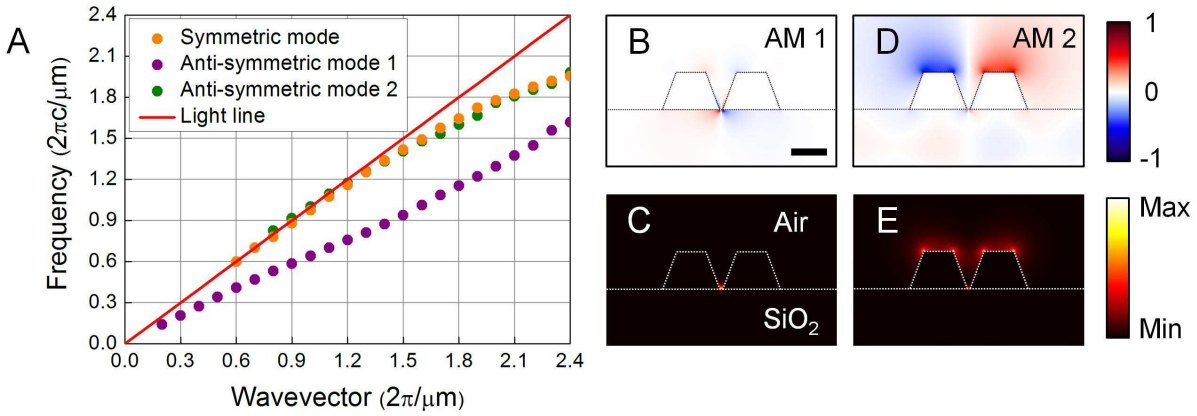

Figure S3. Calculated dispersion curves and field profiles of the SPP waveguide modes in the infinitely long double-strip plasmonic waveguide with a gap of 30 nm. (A) Dispersion curves of one symmetric (orange) and two anti-symmetric (purple and olive) SPP waveguide modes. The anti-symmetric modes (AM1 and AM2) show anti-symmetric field profiles in the z-components of their electric fields. The symmetric and anti-symmetric mode 2 are closely located in the dispersion curve. Light line of vacuum was plotted as the red line. The structural parameters of Figures 4A and B were used in this FDTD simulation. (B)-(E) Calculated field profiles of AM1 and AM2 at a wavelength of 850 nm: the z-components of electric fields of (B) AM1 and (D) AM2, and the electric field intensity distributions of (C) AM1 and (E) AM2. The scale bar in (B) is 300 nm.

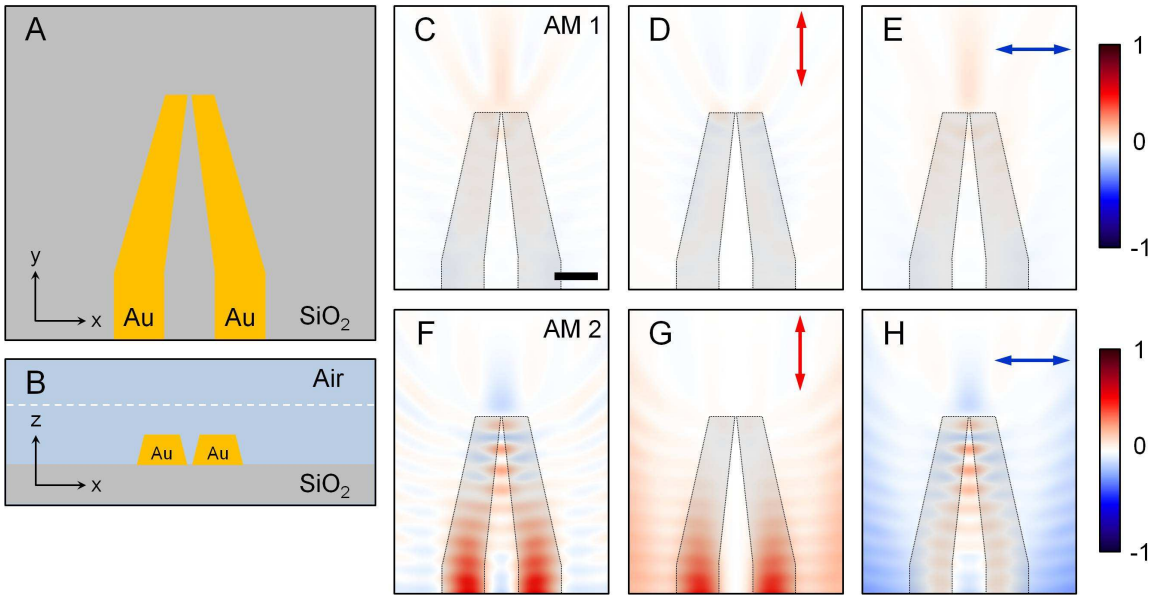

Figure S4. Time-averaged Poynting vector distributions of the two anti-symmetric SPP modes in the double-strip plasmonic waveguide. (A)-(B) Waveguide structure used in FDTD simulation. (A) In this top view, the air gap in the double-strip waveguide gradually decreases from 800 to 30 nm along the waveguide axis (y-axis). The widths of the two strips also decrease from 1000 to 600 nm in the tapered section with a length of 3.5 μm. These structural parameters were considered at the bottom of the waveguide. (B) The cross-sectional view at the tapered end of the waveguide. (C)-(H) The z-components of the time-averaged Poynting vector distributions for the anti-symmetric modes 1 and 2 (AM1 and AM2). The Poynting vector distributions were obtained at a position 400 nm above the top surface of the waveguide, as indicated by a white dotted line in (B). In AM1 and AM2, the z-components of (C and F) total, (D and G) parallel-polarized, and (E and H) perpendicular-polarized Poynting vector distributions were calculated, respectively. The scale bar in (C) is 1 μm. In Figures S4C-H and 4C-E, the identical intensity color bars were used for comparison. We note that the scattered light of the anti-symmetric modes undergoes destructive interference at the gap center of the waveguide (Figure S3B and D). Therefore, the emissions of AM1 and AM2 are negligibly weak at the end of the waveguide, in contrast to the strong focused light spot by the symmetric SPP mode (Figure 4C). Furthermore, the AM1 is attenuated quickly due to the absorption loss of the adhesive chromium layer between the gold waveguide and SiO_2 substrate (Figures S3B and C). Taken together, only symmetric SPP waveguide mode can be observed in our plasmonic waveguide.

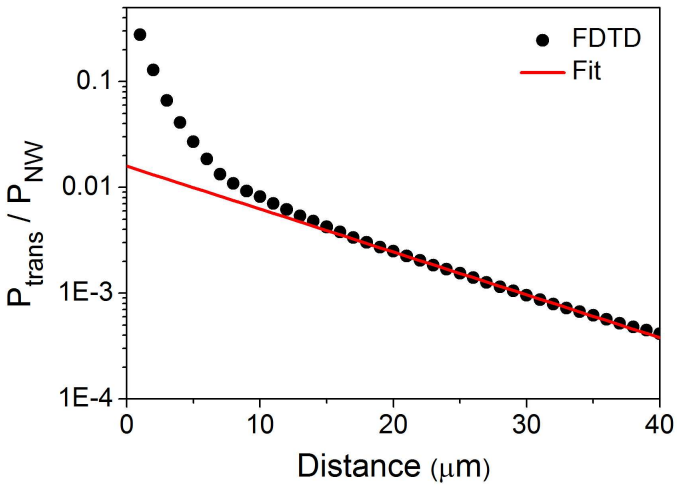

Figure S5. Calculation of the coupling efficiency between the NW LED and the double-strip plasmonic waveguide. We calculated the transmitted powers (P_{trans}) along the waveguide and the total power of the NW (P_{NW}) by using the flux of the Poynting vectors passing through the surfaces including the waveguide and the NW, respectively. The normalized transmitted powers (P_{trans}/P_{NW}) of the symmetric SPP waveguide mode were plotted as a function of the distance from the end of the waveguide coupled to the NW (black dots). At the distance of <15 μm, both direct emission from the NW and coupled light to the waveguide are included in P_{trans}. At the distance of >15 μm, the direct emission from the NW is negligible and P_{trans}/P_{NW} decreases exponentially due to the metallic absorption loss in the waveguide. By fitting P_{trans}/P_{NW} for the range from 20 to 40 μm (red line), the propagation length of the symmetric SPP waveguide mode is estimated to be ~10.6 μm. In addition, the coupling efficiency of the light emission from the NW to the SPP waveguide mode is calculated from the extrapolated value of the red line at the distance of zero, which is ~1.6%. The difference between the black dots and red line indicates the direct emission from the NW.

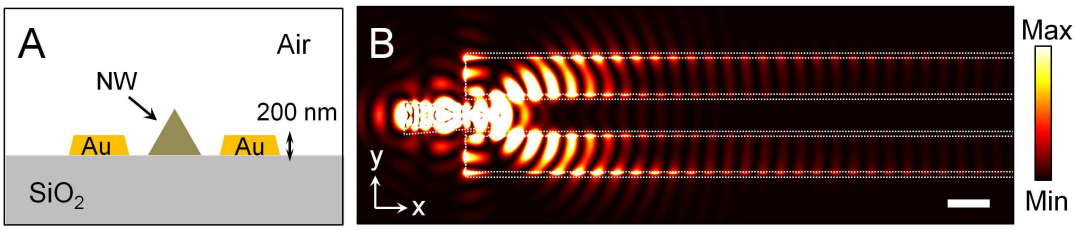

Figure S6. Light coupling from the NW LED to the plasmonic waveguide with a reduced thickness. (A) Side view of the calculation structure. The thickness of the waveguide was set to 200 nm. The other structural parameters are identical to those in Figure 5. (B) Calculated electric field intensity distribution. The light emission from the NW LED was more efficiently coupled to the symmetric SPP waveguide mode excited on the top surface of the waveguide, and as a result, coupling efficiency was increased to ~2.8%. The scale bar is 1 μm.